

Fire microfacies and pyroresidues tracing atmospheric electrification impacts on the Moche Valley and on the Mochica (North Peru)

Microfacies de fuego y piroresiduos como traza de impactos por electrificación atmosférica en el valle de Moche y en los Mochicas (norte de Perú)

Marie-Agnès Courty^{1,*}

¹ PROMES UPR 8521 CNRS, Universitat de Perpinyà Via Domícia, Tecnosud, 66100 Perpinyà, France.

* Corresponding author: (M.A. Courty)
marie-agnes.courty@promes.cnrs.fr

How to cite this article:

Courty, M.A., 2022, Fire microfacies and pyroresidues tracing atmospheric electrification impacts on the Moche valley and on the Mochica (North Peru): Boletín de la Sociedad Geológica Mexicana, 74 (3), A060622. <http://dx.doi.org/10.18268/BSGM2022v74n3a060622>

Manuscript received: January 10, 2022.
Corrected manuscript received: April 15, 2022.
Manuscript accepted: June 9, 2022.

Peer Reviewing under the responsibility of Universidad Nacional Autónoma de México.

This is an open access article under the CC BY-NC-SA license (<https://creativecommons.org/licenses/by-nc-sa/4.0/>)

ABSTRACT

The effects of environmental events on living conditions during occupation periods are studied by comparing alluvial soils and occupation floors that formed during the late Holocene in the Moche valley (North Peruvian coast). The microcontextual study comprises (1) microsurface identification in the field; (2) micromorphological analysis of thin sections; (3) multi-scale characterization of soil components based on digital stereo microscope and scanning electron microscope analysis. The alluvial sequence consists of a 6 m thick alternation of organic silty-clay, fine sandy strata with well-preserved ashy charcoal strata and massive grey sandy beds. This cyclical pattern reflects alternation of stable episodes with a dense reed-bed vegetation, regularly affected by wildfires and drought marked by sand invasions from coastal dunes during El Niño events. The ¹⁴C dates show that these contrasting conditions lasted for one millennium up to establishment of the Mochica empire at the Huaca at 300 years cal. BC. Vesicular slags produced by flash-melting of the soil components, biosourced quartz and nanostructured polymers formed from flash-ionization of the reed vegetation, all with FeCrNi metals coatings, were retrieved in the fired surfaces. They trace impact at the soil surface of electrically charged particles, lightning-flashes, nanoaerosol production by enhanced atmospheric electrification, i.e., flash-heating, shock vaporization, plasma-polymerization of the vegetation and the host matrix. The study shows the occurrence in the basal Uhle platform occupation deposits at the foot of the Huaca de la Luna of similar cemented ashy microfacies associated with a funerary deposit with food offerings in ritual vessels and an intriguing scoriaceous slag. The evidence for ritual disposal of imperishable offerings to deaths is interpreted as the memorial record of the Mochica knowledge of long-lived materials produced by lightning-triggered plasma processes. This integrated study of the environmental and cultural contexts refutes previous assumptions of long-term engineering of the arable alluvial plain to counteract sand invasion and torrential floods. In contrast, the establishment of the Moche pyramids is shown to have occurred during a period of floodplain stability marked by high-energy natural events and lightning processes that offered access to durable soil resources of important social values.

Keywords: microcontextual, aerosol, lightning, plasma, flash, heating, polymerization, preservation.

RESUMEN

Se estudia los efectos de los eventos ambientales para las condiciones de vida durante los periodos de ocupación, comparando los suelos aluviales y los pisos de ocupación que se formaron durante el Holoceno tardío en el valle de Moche (costa norperuana). El estudio microcontextual comprende (1) la identificación de la microsuperficie en el campo; (2) el análisis micromorfológico de secciones delgadas; (3) la caracterización multiscale de los componentes del suelo a partir del análisis con estereomicroscopio digital y microscopio electrónico de barrido. La secuencia aluvial consiste en una alternancia de 6 m de espesor de arcilla limosa orgánica, estratos arenosos finos con estratos de carbón vegetal ceniciento bien conservados y lechos arenosos grises masivos. Esta alternancia refleja episodios estables con una densa vegetación de cañaveral, afectada regularmente por incendios forestales que se alternan con sequías e invasiones de arena de las dunas costeras durante los eventos de El Niño. Las fechas de ¹⁴C muestran que estas condiciones contrastantes duraron un milenio hasta el establecimiento del imperio Mochica en la Huaca en 300 años cal. AC. En las superficies impactadas se recuperaron vesicular-esoriáceos producidas por la fusión instantánea de los componentes del suelo, cuarzo de origen biológico y polímeros nanoestructurados formados a partir de la ionización instantánea de la vegetación de caña, todos ellos con recubrimientos de metales FeCrNi. Se rastrea el impacto en la superficie del suelo de la carga de partículas, los relámpagos, la producción de nanoaerosoles por electrificación atmosférica mejorada, es decir, el calentamiento por destellos, la vaporización por choque, la polimerización por plasma de la vegetación y de la matriz anfitriona. El estudio muestra la ocurrencia en los depósitos de ocupación de la plataforma basal Uhle al pie de la Huaca de la Luna de una microfacies cenicienta cementada similar asociada a un depósito funerario con ofrendas de alimentos en vasijas rituales y a una intrigante escoria vesicular. Este depósito ritual de ofrendas de larga duración a los muertos se interpreta como el registro conmemorativo del conocimiento Mochica de los materiales de larga duración producidos por procesos plasmáticos desencadenados por el rayo. Este estudio integrado de los contextos ambiental y cultural refuta las suposiciones anteriores sobre la ingeniería a largo plazo de la llanura aluvial cultivable para contrarrestar la invasión de arena y las inundaciones torrenciales. Por el contrario, se demuestra que el establecimiento de las pirámides Moche se produjo durante un periodo de estabilidad de la llanura aluvial marcado por eventos naturales de alta energía y procesos de iluminación que ofrecían acceso a recursos de suelo duraderos de importantes valores sociales.

Palabras clave: microcontexto, aerosol, rayo, plasma, destello, calentamiento, polimerización, preservación.

1. Introduction

Evaluating how instantaneous natural phenomena triggered by external or terrestrial causes would have occasionally exerted a major threat on the living conditions of ancient societies remains so far a key challenge (Courty *et al.* 2008; DeMenocal 2001; Bunch *et al.*, 2012; Boslough *et al.* 2012; Wolbach *et al.* 2018; Holliday *et al.* 2020; Bunch *et al.*, 2021). This refined knowledge of past critical situations at the finest temporal and spatial scales is greatly expected to better predict the consequences in a near future of accidental extreme events that could be accelerated by the ongoing climate warming (Bell *et al.*, 2018; Swain, 2020; Tierney *et al.*, 2020). In the last five years, the marked increase of uncontrolled megafires in Australia, USA and Siberia was observed to have rapidly propagated across long distance by intense lightning (AghaKouchak *et al.*, 2018; Tedim *et al.*, 2018; Khaykin *et al.*, 2020). This coupled effect that has remained so far unexplained has incited to question the exact linkages between accumulation of electrostatic charges on vegetation cover and enhanced flammability of the related biomass fuel (Veraverbeke *et al.*, 2017). The common occurrence of vitrified pyrolytic residues in archaeological firing-assemblages has been recently suggested to trace past episodes of enhanced atmospheric electrification as a consequence of high dust loading (Courty *et al.*, 2020). Effects of triboelectricity in highly turbulent volcanic plumes on the aggregation of charged fine aerosols and on the production of glass by fusion has been well documented and experimentally reproduced (James *et al.*, 2008, Gaudin and Cimarelli, 2019). Similar mechanisms of charge production from high-energy collisions would likely occur in the megafire stratospheric carbonaceous vortex that has been recently identified (Khaykin *et al.*, 2020). Charging processes and nanoaerosol formation caused charging by dust exposure to cosmic radiation are known to be involved in pulses of atmospheric electrification, possibly in lightning, but the exact links are not yet fully understood (Lushnikov *et al.*, 2014; Izhovkina

et al., 2020). In the absence of a robust present-day database on the impact at the Earth's surface of charged aerosols produced by electrification pulses, their possible occurrence in the past has been so far ignored. Most studies dealing with past records of atmospheric electricity fluctuations have focused on the formation of fulgurites by lightning-strikes. The distinctive tubular glassy morphology due to local flash-fusion along the electric discharge pathway in quartz sands with their unusual minerals has been for long been an object of fascination (Grapes and Müller-Sigmund, 2010; Pasek and Pasek, 2018), whereas the glassy vesicular materials formed in clay soils have not received the same attention (Gifford, 1999). However, the scarcity of fulgurites in ancient or present-day environments and their more common occurrence in sandy deserts show that these are only incidental footprints of electrification processes. These curiosities are obviously insufficient for tracing in past or recent soils effects of atmospheric electrification that presently occurs throughout the entire planet with an average frequency of 44 lightning-flashes per second, mainly over land areas (Christian *et al.*, 2003).

The effects of atmospheric electrification have been for long known to be strongly constrained by air moisture content, aerosol ionization and dust electrical charging in the lower atmosphere (Harrison *et al.*, 2020; Liu *et al.*, 2021). Electric arc explosion would convert air to species such as O₃ and NO_x with production of abiotically fixed nitrogen in the lightning channel air and potential greenhouse effect (Nna Mvondo *et al.*, 2001; Babrauskas, 2018). Nitrogen liquefaction in the lightning discharge could even form polymer walls of wax on the channel in the presence of carbonaceous aerosols (Bychkov, 2002). It is also well established that the soil moisture content and the properties of the host-materials control the propagation of the lightning conductive channel at and within the soil surface (Pasek *et al.*, 2012; Kim *et al.*, 2016). The complexity of these controlling parameters explains why the vertical pathway with the resulting tubular fulgurite is simply

an exceptional pattern of weak environmental relevance. In fact, the effects of the considerable energy deposition of lightning into the target soil surface are similar to the ones of hyper-velocity impacts, but more local in spatial extent and more ubiquitous (Feng *et al.*, 2019). Vaporization of aerosols, vegetation and organic compounds is expected to produce filamentary aggregates from the charged gas-suspended particles acting as electric dipoles (Abrahamson and Marshall 2002). The lightning strike fusion would lead to silicate liquid immiscibility, production of metal droplets by extreme reduction and spatial spreading of the flash-melted droplets by the electric arc explosion (Essene and Fisher, 1986; Babrauskas, 2018; Feng *et al.*, 2019).

Our pioneering exploration on these challenging issues have allowed to identify in diverse archaeological contexts a range of polymeric components formed from aerosols and/or soil organic components by lightning-triggered plasma processes (Courty *et al.*, 2012, Courty and Coqueugniot, 2013; Courty, 2017; Courty *et al.*, 2020). With these diagnostic attributes in hands, the next critical step is now to integrate the polymeric components within the microcontextual study of ancient soil surfaces in order to define periods of enhanced aerosol electrification by a distinctive suite of soil microfacies with their relevant assemblage of pyrolytic microresidues and related components. We formerly explained why our previous confusion of these polymeric components with possible impact on the soil surface of extra-terrestrial hyper-velocity bolide collision is at first a question of soil archive quality (Courty *et al.* 2008). Effects at the Earth's surface impacts of lightning events and extra-terrestrial bolide impact share in common sudden air ionization, aerosol plasma processes and hyper-sonic shock-waves (Courty and Martinez 2015; Feng *et al.*, 2019; Murphy, 2020). They would obviously differ by the timing of flash-related processes and the related spatio-temporal patterns of their specific effects at local to regional scales. The distinction between the two types of high-energy atmospheric

phenomena would at first imply to perform a meticulous high-resolution contextual soil study to search for the preserved records of these super-fast events with their complex spatio-temporal patterns (Courty, 2018). Unfortunately, the ongoing debate on the sedimentary records and microresidues assemblage of hypothetical catastrophic Tunguska-class airbursts prefers to ignore the basic principles of microcontextual study of natural soil sequences or occupation deposits of archaeological sites (Moore *et al.*, 2020; Bunch *et al.*, 2021).

We present here the simple case study of the Moche valley in northern Peru that integrates within a small region a floodplain sequence and the occupation deposits at the Huaca de la Luna. This dual study is aimed to further explain the innovative microcontextual methodology that has to be performed for elucidating the exact nature and the spatio-temporal pattern of exceptional firing events triggered by enhanced atmospheric electrification.

2. Materials and methods

2.1. THE STUDIED CONTEXTS

The study area belongs to the flat littoral fringe of the North Peruvian coast (Figure 1a) that is hyper-arid with less than 20 mm of rain per year. The rain shadow effect of the Humboldt Current along the Pacific coast of South America maintains desert conditions on the landscape formed of sand levees and large dune fields. This extensive flat sand blanket accumulated from deflation of the continental plateau during the late Pleistocene marine regression.

In the Moche Valley, annual temperatures average 20° Celsius, with approximately 4 mm of precipitation near the ocean to approximately 30 mm near the Andean foothills (ONERN, 1973). The occasional precipitation is sustained in part by a layer of low hanging cloud fog that is created when dry winds hit the lower western slope of the

Andes. The Moche hydrographic regime is controlled by seasonal variations of heavy rainfall over the upper catchment basin in the Occidental Cordillera of the Andes at 4000 m altitude. The rather overall stability of the braided, weakly incised river bed in the lower floodplain is considered to have been initiated at about 3,000 years ago (Sandweiss and Richardson, 2008). The El Niño Southern Oscillation (ENSO) is known to have occasionally triggered extreme weather phenomena known as the El Niño events throughout the prehispanic era up to the present period (Waylan and Caviedes, 1986). The extensive heavy rains that are caused by the warm oceanic currents have repeatedly led to turbulent flooding and severe erosion of the levelled pampas formed of complex colluvial-alluvial deposits from the Cretaceous granodiorite out-crops. Low to moderate El Niño events occur every 2–8.5 years (Rodbell *et al.* 1999), whereas more extreme events occur approximately every 15 years. In the twentieth century, the most recent severe El Niño events occurred in 1925–1926, 1982–83 and 1998–99. This latest severe El Niño event deeply impacted the agricultural lands with considerable soil loss marked by a deep incision throughout the lower alluvial plain. This extensive vertical entrenchment has offered a unique oppor-

tunity to examine long catena with fresh sections of the late Holocene deposits downstream to the ‘Cerro Blanco’ hill, just at the foot of the Moche archaeological complex (Figure 1b).

In the northern coastal region of Perú, the Mochica people occupied contrasting environments in the lower elevations of the Andes (0–500 masl) and adjusted to natural constraints by landscape conversion from coarse-grained desert outwash to fine-grained arable floodplain (Goodbred *et al.*, 2020). Their increased urbanism and social complexity with construction of the grand pyramids and massive expansion of agricultural capacity is assumed to have emerged through large-scale irrigation technology (Dillehay *et al.*, 2004).

The Mochica sequence in the great pyramids of the Moche valley, has however shown recurrent invasions of aeolian sands, possibly linked to El Niño events along to the 800 years occupation (Chauchat *et al.*, 2021): Moche I and II (100–200 AD), Moche III (200–450 AD), Moche IV (450–650 AD) and Moche V (650–800 AD). Evidence for irrigation canals bringing the Andes precipitation from the upper inland was only encountered during this ultimate Moche occupation phase (Chauchat *et al.*, 2021). El Niño events are interpreted to have shaped Moche cosmologies and



Figure 1 Location of the study area. 1a. Location of Huacas de Moche site along the Pacific Ocean coast, north Peru. 1b. Location of the two studied contexts, the Moche valley (brown circle), the Moche archaeological site with the Huaca del Sol and Huaca de la Luna.

rituals, possibly reflected in particular themes of the Moche iconography related to human sacrifice and death as well as animals and plants (Bourget, 2016). A possible link between a large El Niño event and the collapse of the Moche urban center was debated (e.g., Kolata *et al.* 2000; Moseley *et al.* 2008).

The excavation performed for eleven field seasons in the Uhle platform that is located at the foot of the western façade of the Huaca de la Luna has allowed to document the evolution of the monumental architecture and the associated human activities in this part of the Moche site (Chauchat *et al.*, 2008; 2021). The platform (57 m long, 25 m wide, and 2-3 m high) is associated to marginal areas on all four sides, including a group of dwellings to the southwest, a large enclosed plaza to the north, and a space at the foot of the Huaca to the east. This area was identified to have been at first a place of public activities (Moche phase I), probably of worship to a stone idol whose piece was found, with various rituals such as pilgrimages. From Moche phase II, the platform turned to be exclusively devoted to funerary practises with a complex pattern of tombs. The excavation of 57 tombs has revealed a great variety of forms, offerings and remains of funerary rituals, with well-preserved human remains, animal offerings, personal objects and high quality ceramics. In its final stage, the excavation exposed at the base of the Uhle platform an empty, non-constructed space with a well-preserved occupation complex that strongly contrasted from the loose, sandy activity layers of Moche phases I-II, III and IV. The lateral section showed that this thick occupation complex (designated as layer 21 D occupation complex) rested directly on the sandy substratum corresponding to the dune formations that covered the rocky base, before the construction of the monumental architecture of the early Moche I phase. The excavation of the upper 30 cm of layer 21 D complex has not allowed to comprehensively explore the lowermost occupation sequence.

The occupation complex showed the spatial association of massive, densely compacted, green-

ish microstratified, ashy sandy silt and the fine interstratification of bow-shaped microstratified ash lenses. The abundance of unusual coarse-textured ceramic fragments and the dense assemblage of crushed bones all showing *in situ* fragmentation suggested to consider the ashy deposit as feast remains and repeated ritual offerings. A meticulous surface cleaning of the occupation complex revealed the occurrence of a vesicular slag, a unique object of this kind so far encountered in pre-Hispanic archaeological contexts of South America. Facing the impossibility to properly excavate this remarkable occupation complex for logistic reason, a microcontextual study of the puzzling slag and of the microstratified deposits was performed in order to further test their cultural and environmental relevance.

2.2. FIELD SURVEY, SAMPLING AND ANALYTICAL STRATEGY

A systematic field survey of the fresh sections that were accessible throughout the lower floodplain was performed in order to sketch the spatial variability of the exposed sequences. Considering the sharp contrast between the microstratified dark brown organic-rich strata and the homogeneous sandy and silty-clay massive units, great care was devoted to define at the finest spatial scale the lateral extent of each individual microstrata by following its lower and upper limit. The vertical section exposed at the Pampa del Cacique location was showing the most complete record with deep exposure of the lower microstratified dark brown strata with charcoal-rich lenses. This sequence was selected for sampling a series of ten undisturbed blocks (Figure 2b, Table 1). This discontinuous column devoted to the preparation of thin sections was performed in the core of homogeneous sandy facies and at distinctive boundaries for the microstratified ones. While cutting the blocks, 100 g of bulk sediments was sampled for a selection of microstratigraphic units that were defined by their sharp lower and upper limits on the freshly exposed cuts. The microfacies integrity of the bulk samples was

Table 1. Moche valley stratigraphic sequence.

Stratigraphic units	Microfacies	Diagnostic features and components
Unit IV 150 -220 cm Moche and Chimú pottery sherds	Massive, weakly layered yellowish grey silty sand with discontinuous yellowish brown silty clay and dark brown carbonaceous lenses	Loose packing to incipient channel microstructure; weakly expressed bioaggregation along root channels
Unit IIIb 35-60 cm	Micro-stratified grey silty sand, yellowish brown silty clay and dark brown carbonaceous laminae with char lenses	Fine fissural microstructure. Lenses with abundant reed charcoal, vitrified charred reed, polymer films and filaments, polymerized reed fragments, baked-clay aggregates, carbonaceous aggregates, metal-splashed angular quartz and vesicular slags
Unit IIIa 50-75 cm Diffuse upper limit	Interstratification of finely-layered grey silty sand, massive yellowish brown silty clay and micro-stratified, carbonaceous microfacies	Fine fissural to massive microstructure Common metal-splashed angular quartz, polymerized baked-clay aggregates, charcoal with polymer films and filaments
Unit II 110 -150cm Sharp upper limit	Homogeneous finely layered silty sand	Massive to fissural microstructure. Subangular to subrounded sands
Unit Ib 75-135 cm Diffuse upper limit	Interstratification of finely-layered grey silty sand and dark brown carbonaceous with charcoal laminae	Massive to fissural microstructure. Subangular to subrounded microstructure calcium sulphate crystals, reed charcoal; polymerised reed fragments; rare metal-splashed angular grains.
Unit Ia 30-45 cm Sharp upper limit Bottom not reached	Densely compacted, composite micro-stratified microfacies : dark brown carbonaceous with charcoal laminae, dull orange clay, yellowish brown silty sand	Fine fissural microstructure Abundant angular calcium sulphate crystals, reed charcoal; polymerised reed fragments; charred, calcined and polymerised phytoliths; polymer filaments and films; metal splashed angular quartz and baked clay-aggregates.

controlled by performing surface excavation on restricted surfaces from the exposed section. In addition to this benchmark sequence, complementary bulk samples were collected at locations showing microfacies variability of colour, texture, abundance of vesicular glassy coarse components and of pyrolytic residues.

In the layer 21 package D occupation sequence of the Moche site, three small-sized undisturbed blocks were collected in the microstratified, ashy sandy silt in addition to bulk samples by individual microstrata, whereas only bulk samples were collected within individual microstratified ash lenses due to the overall lack of cohesion and the high density of artefacts.

Thin sections were prepared from the blocks and studied under the petrographic microscope

following the principles and terminology adapted from sedimentary petrography (Humbert 1972) and soil micromorphology (Bullock *et al.* 1985, Courty *et al.* 1989).

The bulk samples were wet sieved to produce residues of above 2 mm, 2–1 mm, 1 mm–500 µm, 500–250 µm, 250–100 µm. Soaking in warm water and intense washing was performed to obtain complete disaggregation. The morphology, structure, degree of cementation and compositional range of mineral, organo-mineral and organic components were meticulously examined by reflected light under a digital stereoscopic microscope (DSM) as water-suspensions and as dry residues. Successive observations were performed at different stages of disaggregation in order to keep the filiation between the coarse components of the aggregates and of

the fine matrix which is irreversibly lost during the water-sieve. This was devoted to control the link between the diverse pyroresidues (charcoal, char fragments, phytoliths, ash components), the unburnt plant remains, the minerals and the polymerized components (films, filaments and composite aggregates). For the later, a particular attention was devoted to identify the distinctive characteristics of plasma-discharge products, *i.e.* nanostructuration and metal inclusions as previously defined (Courty, 2017; Courty *et al.* 2020). The identification of the polymer nanostructuration and of the type of nanostructured metal pattern was studied using a Hitachi 4500 scanning electron microscope under low vacuum and in backscattered electron mode from a selection of grains.

^{14}C AMS dating was performed on a selection of charcoal-rich lenses after confirming from

observation under the DSM, their well-preserved plant structures, the lack of vitrification, *in situ* breaking from coarse fragments and the lack of contamination by fine root deep-penetration.

3. Results and interpretation

3.1. THE MOCHE LOWER FLOODPLAIN SEQUENCE

3.1.1. MICROFACIES

The deeply incised section exposed by the 1999 El Niño flood along the present bed of the Moche river has allowed to observe a 4 to 6 m sequence showing two distinctive depositional periods (Table 1). At the bottom, the regularly stratified fine textured deposits with weak signs of pedogenesis, only marked by iron staining along desiccation fissures and incipient bioturbation, are typical of

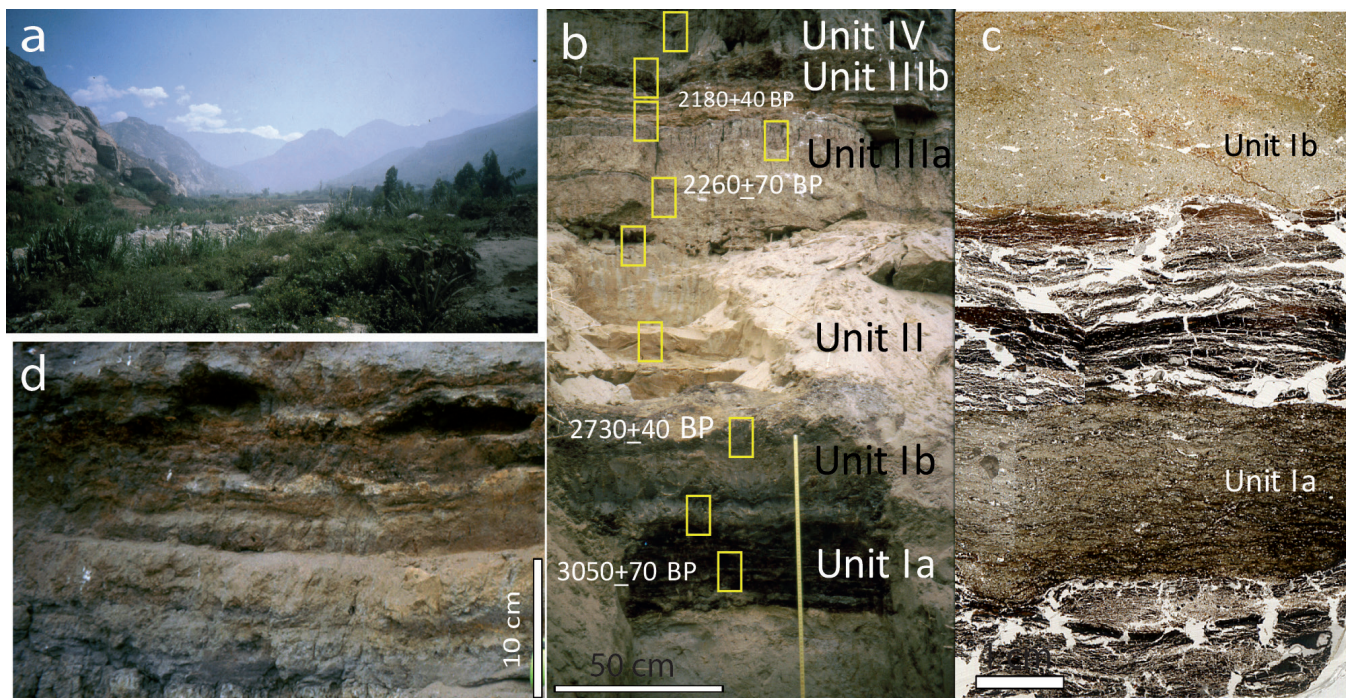


Figure 2 Field view of the studied sections in the Moche valley and scan view of the microfacies. 2a. View of the Moche river when springing out from the Andes hills in the coastal plain showing incision of the present braided bed with accumulations of boulders and cobbles. 2b. Stratigraphic sequence of the late Holocene floodplain deposits at the Pampa del Cacique (Conache), upstream of the Huacas de Moche site showing alternation of carbonaceous brownish-black silty-clay microstratified facies and water-reworked aeolian sand deposits. 2c. Scan view of the contact between the microstratified brownish-black silty-clay Ia deposits and the Ib water-laid aeolian sands. 2d. Close view of the contact between the IIIa massive silty clay and the IIIb carbonaceous microstratified facies showing interstratified lenses of reddish brown silty clay, silty sands and dark grey carbonaceous laminae.

a low energy alluvial environment. In contrast, the upper part displays a coarse texture, a poorly expressed stratification and a weak horizonation with fine textured slaking crusts at strata interface. This succession of pedo-sedimentary facies indicates a deposition from repeated destabilisation episodes of the surrounding foothills and aeolian input from the coastal sand dunes, interrupted by episodes of incipient soil development. The rare transverse section to the valley axis has shown that the upper colluvial deposits lies in sharp discontinuity on massive, clay-rich colluvium that are intensely bioturbated with well-expressed iron segregation along root channels. We previously reported that the massive clayey colluvium deposited during the mid-Holocene and suffered severe erosion at ca. 4 kyr BP in response to an abrupt environmental change (Courty *et al.*, 2008). The lower Ia finely stratified alluvial deposits can thus be understood to express the restoration of a stable floodplain following the drastic mid-Holocene landscape disruption. In spite of in-depth refreshment of the existing section, the bottom of the Ia deposits could not be reached. It is highly plausible that it does not represent the very initial phase of the late Holocene floodplain restoration. The possibility of an incomplete depositional record has however no major implication for debating the environmental relevance of the exposed floodplain microfacies.

The systematic field survey along the exposed section of the lower floodplain sequence has allowed to observe the remarkable homogeneity of the regularly stratified lower deposits, without evidence of lateral channel incision from the adjacent foothills. The common association of charcoal lenses to the finely laminated carbonaceous microfacies in the I and II microstratified units incites to consider this sequence as the record of cyclical firing events. In the absence of hearths, of combustion facies that are typical of local *in situ* firing or of human artefacts throughout the lower sequence (units I to III), the carbonaceous microfacies are hypothetically attributed to natural wildfires. This is also with the lack of human artefacts that were only coherent in the sequence

at strata interfaces of the colluvial unit IV as scattered rounded sherds with paste characteristics similar to Chimu and Moche ceramic assemblages (Lockard, 2009). The depositional regularity of the firing microfacies and their wide spatial extent across the valley also refute the possibility of pyroresidues accumulations produced by repeated slash-and-burnt activities in the floodplain.

The restricted excavation that was performed for controlling the integrity of microstrata while collecting bulk samples has shown the common occurrence of infra-millimetre-thick surface hardening. This type of distinctive interface appeared to contrast from the one only encountered in the upper part of unit III formed of microstratified crusts with lenses of centimetre-sized vesicular granules looking similar in the field to the ones of the Middle Holocene sequence (Courty *et al.*, 2008).

Based on the radiocarbon datings, the depositional history of the lower floodplain sequence represents an approximately 1000 years long period during an early phase of the upper Holocene. (Table 2). The clearly different ^{14}C ages allow to tentatively propose that unit I experienced a series of wildfires for ca. 300 years, whereas similar conditions were recorded for ca. 1000 years during the deposition of unit III. The four radiocarbon ages are obviously not sufficient to exactly estimate the duration of the different firing episodes. However, the dating coherence provides solid support to further scrutinize the relevance of the related microfacies in terms of firing events and depositional conditions of the associated pyroresidues.

In the continuity of the field observations, the micromorphological study of the thin sections that was performed under the petrographic microscope has allowed to identify the repeated occurrence in units I and III of diverse firing microfacies with singular characteristics (Figure 3). The composite microfacies with their repeated alternation of three distinctive types of lamina (Figure 3a) corresponds to the ones that were showing in the field a hardened surface at the top of the dull orange clay laminae. The sharp interfaces and the integrity of each lamina with their distinctive composition

Table 2. ¹⁴C radiocarbon datings of the Moche valey alluvial layers and of the Uhle platform occupation contexts.

<i>Moche Valley sequence</i>						
Reference	sample	Measured radiocarbon age	¹³ C/ ¹² C ratio	Conventional radiocarbon age	2σ calibrated results (95% prob. BC)	2σ calibrated results (95% prob.) BP
PE01-CA14B Unit IIIa2	AMS Beta-146588	2060±40 BP	-17.6‰	2180±40 BP	370-110 BC	2320-2060
PE01-CA14 Unit IIIa1	Standard Beta144303	2240±70 BP	-23.8‰	2260±70 BP	410-165 BC	2360-2115
PE01-CA19 Unit Ib	Beta-155391	2750±40 BP	-26.1‰	2730±40 BP	940-810 BC	2890-2760
PE01-CA26 Unit Ia	Beta 155392	3080±70 BP	-27‰	3050±70 BP	1440-1100 BC	3390-3050
<i>Uhle platform, Moche site</i>						
Reference	sample	Measured radiocarbon age	¹³ C/ ¹² C ratio	Conventional radiocarbon age	2σ calibrated results (95% prob. BC)	2σ calibrated results (95% prob.) BP
63EL7N4 Huaca de la Luna, lower level. Phase I	Gif 11825	1526±35 BP	-25.86‰	1520±35 BP	430-635AD	1520-1315
Moche N°1: 75.70 m Ash layer	Gif-11964	1960±50 BP	-17,54‰	1980±50 BP	33 BC:31 BC 20 BC:12 BC 1 BC:237 AD	2120-1800
PE2001-2 N°1: 75.56 m	Gif-11965	1585± 30	-20,34‰	1590± 30	432 AD:601AD	1518-1349
PE2001-3 N°1: 75.60 m	Gif-11966	2005±70	-23,44‰	2050±70	153:139 BC 113 BC:235AD	2103-1715

and texture are typical of low-energy water-deposition (Courty, 1995). Each individual composite microfacies represents a three-fold depositional cycle that comprises from the bottom to the top (1) the yellowish brown silty sand, (2) the dark brown carbonaceous silt with charcoal fragments and (3) the dull orange clay. Based on its texture and composition, the lamina type 2 would correspond to a water-deposition of fresh pyroresidues soon after the firing-event. The close association of lamina type 3 to the type 2 indicates that the firing event was rapidly followed by an episode of fine aerosol input under calm depositional conditions. In contrast, the coarser texture of lamina type 1 would express subsequent reworking by gentle runoff of the dual firing-aerosol microfacies, thus diluting in the fine-mass part of the singular aeolian component. However, the sharp undulating lamina type

2/ type 1 interface suggests that the former resisted to the running water due to its hydrophobicity and hard-setting. The thin sections confirm the lack of a cyclical depositional pattern for the firing facies showing in the field a weakly expressed microstratification, lack of distinctive interface and scattered coarse charcoal (Figure 3b, 3c). Their irregular microstratification was formed by the fine interlayering of clay, sandy silt and silty sand carbonaceous laminae with similar characteristics to the previously described ones. This fine imbrication associated to the fresh aspect of the pyroresidues shows that the distinctive laminae were partly homogenized due to water stagnation and low-energy runoff reworking. Although it is impossible to stratigraphically identify each firing event and the subsequent aerosol input, this range of cyclical deposition appears to have most likely occurred.

The only occurrence of *in situ* heating was identified in thin sections near the top of the IIIb microstratified deposits with the finely cracked charred clay domains embedded in the massive carbonaceous fine mass with randomly scattered abundant angular charcoal (Figure 3d). The microlayered slaking crusts with coarse sandy vesicular granules encountered at the interface between IIIb and IV deposits (Figure 3e) helped to identify the fall of exotic materials on the fired surface and local reworking of the pyroresidues by high-energy flooding.

All the diverse firing microfacies identified throughout the sequence thus share in common the close association of pyroresidues to domains or lamina of pure dull orange clays that are tentatively interpreted to be of aeolian origin based on their depositional context. This hypothesis is supported by their marked textural and depositional contrast with the massive silty clay facies encountered in units II, IIIa and IIIb (Figure 3f). The extensive occurrence of the later with their typical characteristics of low energy accumulation and water stagnation shows that the massive silty

clays form the bulk of the local floodplain sedimentation. The absence of pyroresidues indicates that their deposition took place without interference with wildfires in the flood plain.

Similarly, no evidence of pyroresidues was detected in the fluvial unit II that is formed of horizontal to subhorizontally bedded sand-dominated strata with sandy silt laminae.

3.1.2. PYRORESIDUES AND ASSOCIATED COMPONENTS

The DSM observations of the water-sieve sized-residues in the firing microfacies of I and III units has revealed the occurrence of similar pyroresidues and associated components showing the diagnostic features of lightning-related firing as previously defined (Courty, 2017; Courty *et al.*, 2020). They are considered by each contextual unit because the two sets of firing records differ by the type of burnt vegetation and surface firing processes, the depositional settings and the preservation conditions.

During the water sieving, the unit I fired deposits have shown an easy sorting and washing

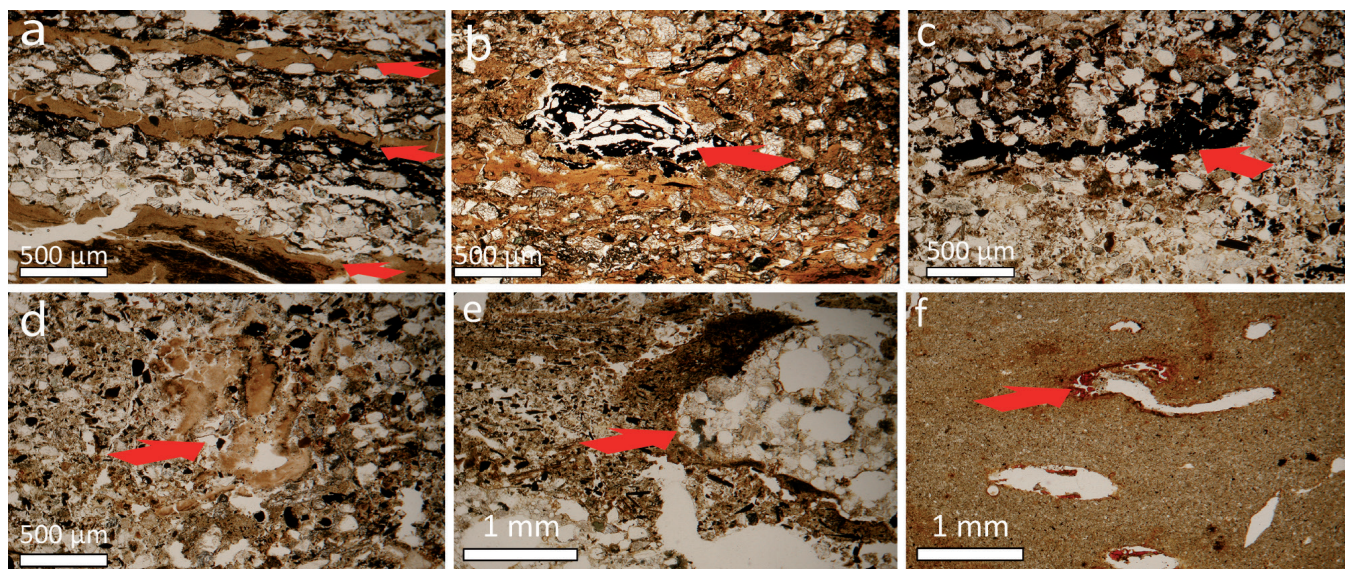


Figure 3 Thin section illustrations of a few representative microfacies. 3a. Regularly microstratified composite microfacies showing alternation of 3 units: dark brown carbonaceous, dull orange clay, yellowish brown silty sand. 3b. Irregularly microstratified dull orange carbonaceous silty clay microfacies. 3c. Irregularly microstratified dark brown carbonaceous microfacies. 3d. Massive yellowish brown carbonaceous silty clay microfacies with cracked charred clay domains. 3e. Coarse sand vesicular granules embedded in yellowish brown carbonaceous silty clay slaking crust. 3f. Massive, homogeneous dull orange silty clay.

of the sand-sized components consisting of quartz grains, calcium sulphate crystals and charcoal, all with dust-free and bright surfaces (Figure 4a). In contrast, a marked hydrophobicity and resisting cementation to gentle hand-mechanical pressures were noticed for the clay-rich and carbonaceous aggregates that were thus abundant in the fine-sand fraction (Figure 4b). Their controlled disaggregation has allowed to extract from the fine mass a profusion of reed fragments showing well-preserved distinctive anatomical structure. A great part of them was lost during the final disaggregation due to their enhanced fragility by the intense warm water washing.

Only the white calcined reed fragments and the ones showing a blue colour, and a bright surface with coating of splashed metal-droplets appeared to be more resistant (Figure 4f). Similar metal coatings were identified on angular quartz grains with sharp edges and on quartzitic breccia with carbonaceous inclusions (Figure 4c). Unburnt organic sand-sized

composite grains formed of densely compacted reed fragments, coated by polymer films with splashed metal-droplets and carbonaceous inclusions showed marked resistance to water sieving (Figure 4d). Blue polymerized phytoliths, vitrified reed charcoal and twisted polymer filaments were extracted from the fine mass after performing ultimate disaggregation by mechanical pressure and hot water sieving (Figure 4e). The SEM analysis has allowed to more clearly identify the micron-thick polymer films with metal and salt inclusions linking the silicified and carbonaceous reed components (Figures 5a-5f) and the incrustations of metal and salt particles within the polymerized blue silicified fragments with degassing vesicles (Figure 5f).

In comparison to the unit I fired deposits, the clay-rich organic and carbonaceous components of the unit III microstrata were more easily disaggregated into elementary particles without evidence of fired or cemented composite grains

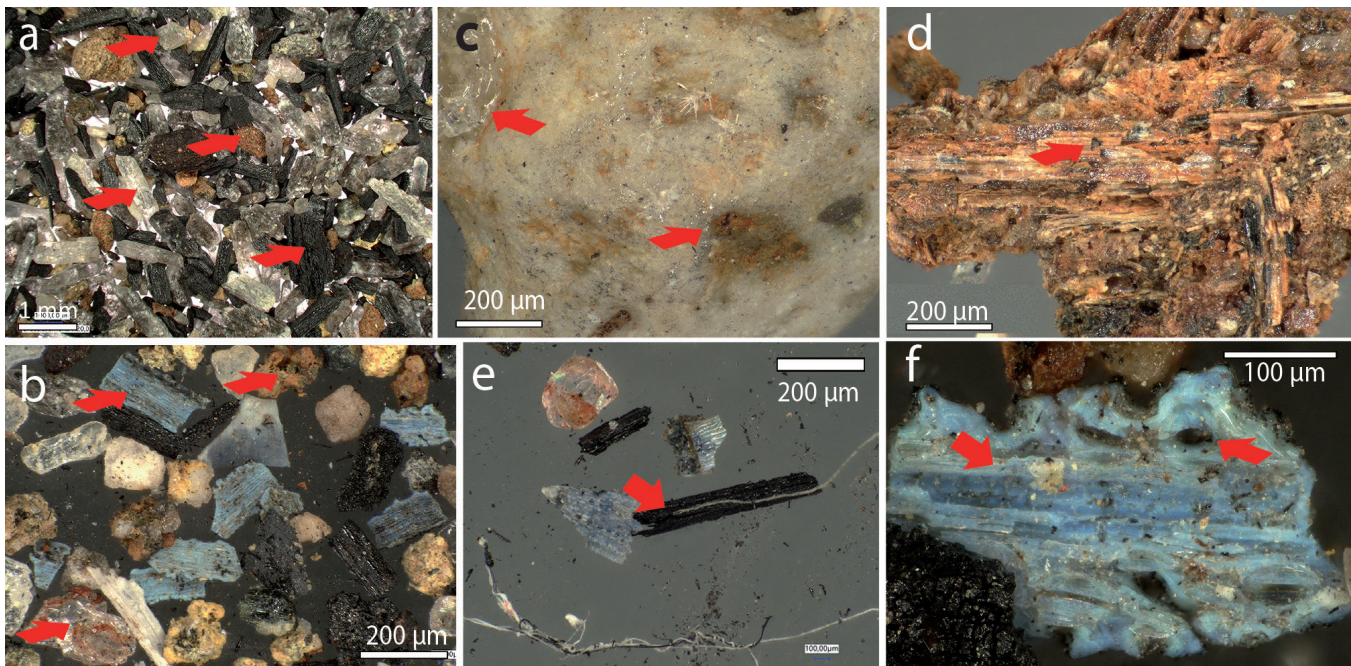


Figure 4 Distinctive features and components of the Ia microstratified carbonaceous facies. 4a. DSM view of the fine sand fraction formed of angular quartz, calcium sulfate crystals, reed charcoal and dark-orange baked clay-aggregates. 4b. DSM view of the most resistant reed fragments consisting of abundant calcined, metal-pulverized and polymerized components with angular quartz and baked clay aggregates. 4c. Detailed DSM view of a quartzitic breccia metal-splashed surface. 4d. Detailed DSM view of a polymerised reed fragment with metal inclusions. 4e. DSM view showing the close association of the blue polymerized phytoliths, vitrified reed charcoal and twisted polymer filaments. 4f. Detailed DSM view of (4b) showing the distinctive plant structure within the blue polymerized.

in the residues. The DSM control during the disaggregation procedure showed the occurrence of polymer films and filaments at the interface between reed fragments and mineral particles of the aggregates (Figure 6a). The filaments resisted well to the mechanical hand pressure and to the water sieving, whereas the films got brittle and disaggregated into acicular flakes, thus losing their distinctive morphology of stacked coloured films. Polymerized carbonaceous elongated aggregates retrieved at carbonaceous microfacies interface showed on one side a dense stacking of partly melted vesicular beads (Figure 6b) with a metal-splashed surface (Figure 6c) whereas the reverse polymerized side was smooth and bright without metal coatings. Under SEM, the vesicular bead

showed a dense stacking of glassy domains and metal coatings sticking to sharp edges of the glassy phases (Figure 6d) with their foliated nanostructure indicating deposition from plasma-jetting of electrically charged droplets (Figure 6f). An origin from partial melting by flash-heating followed by rapid quenching of plant materials mixed with mineral components is deduced from the elongated morphology of the glassy domains, their variable elementary composition at microscale given by EDS analyses, the diversity of mineral grains with sharp edges in the fissures, the occurrence of carbonaceous inclusions (Figure 6e). Although these components were not observed *in situ* when sampling the strata interface, the contrast between the two sides of the polymerized carbonaceous aggregates

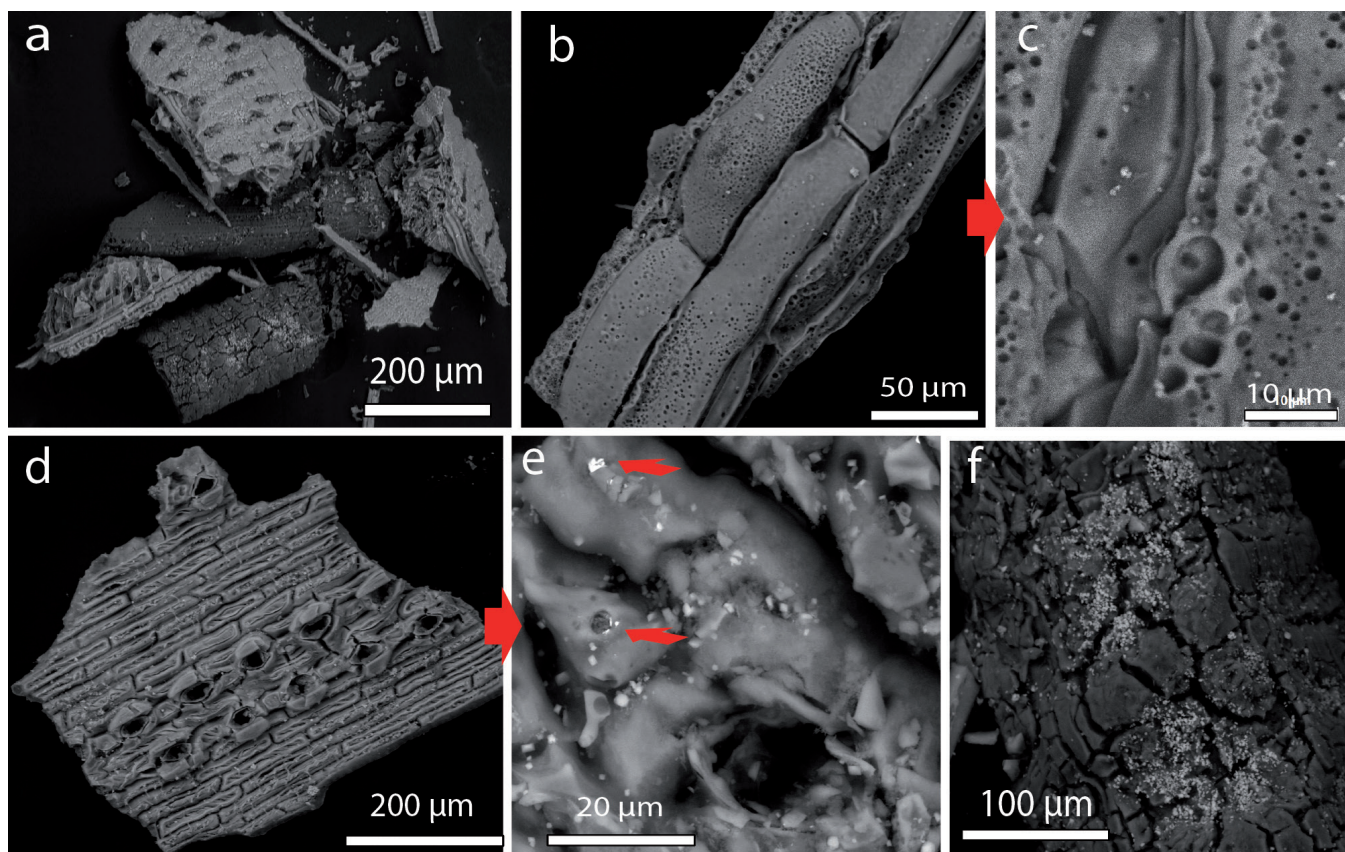


Figure 5 SEM characteristics of the blue polymerized phytoliths (cf. fig. 4). 5a. Resistant aggregate to intense water-sieving, made of silicified and carbonaceous reed fragments with well-preserved anatomical cells, bound by a polymer film. 5b. Well preserved reed fragment showing at high magnification (5c) partial melting and degassing cavities due to flash heating. 5d. Well preserved reed fragment with silica skeleton and stomatal cells showing at high magnification (5e) high concentration of BaSO_4 microparticles tracing refractory residues from flash-vaporisation. 5f. Finely-cracked vitrified reed char produced by flash-heating with encrustation of BaSO_4 microparticles.

suggests the vesicular beads to trace plasma-jetting projection of glassy droplets on the flash-heated soil surface. Similar FeCrNi nanostructured coatings were observed on the sharp edges of coarse angular quartz that contrasted from the dominant subangular to subrounded alluvial sands not showing metal particles at their surfaces (Figures 7a and 7b). The sand-sized water-sieve residues has also showed abundant polymer components formed of twisted filaments (Figure 7c), and stacked films (Figure 7e), with metal inclusions (Figures 7d and 7f) which are both indicating plasma-discharge synthesis (Hamdan *et al.*, 2017).

The association of the singular quartz population to the polymerized aggregates with their glassy droplets suggests that the flash heating caused by the electrically charged plasma-jet locally induced quartz breaking due to surface propagation of the lightning shock-wave. In contrast, the dominant population of TiO₂ microspherules and nanoparticles in the carbonaceous matrix incites to rather consider the foliated films as exotic components

tracing the fall at the fired-soil surface of aerosols that were transformed during their aerial transport by electrification processes. The polymer filaments could share the same aerial provenance although their close association to the locally fired vegetation indicates that they also formed from the flash-vaporized surface by the lightning discharge.

3.2. MICROFACIES, PYRORESIDUES AND RELATED COMPONENTS OF THE UHLE PLATFORM OCCUPATION DEPOSITS

The green coloured microstratified ash deposits of the basal layer 21 package D occupation layers shows a sequence of dark brown organo-mineral beds rich in carbonized residues, thin brown silty-clay lenses with plant imprints, and silty-sandy beds rich in siliceous phytolith-like residues and thin ash lenses (Figure 8).

The excellent preservation of the micro-stratification despite the weak cohesion of the constituent compounds, especially the ashy strata, the absence

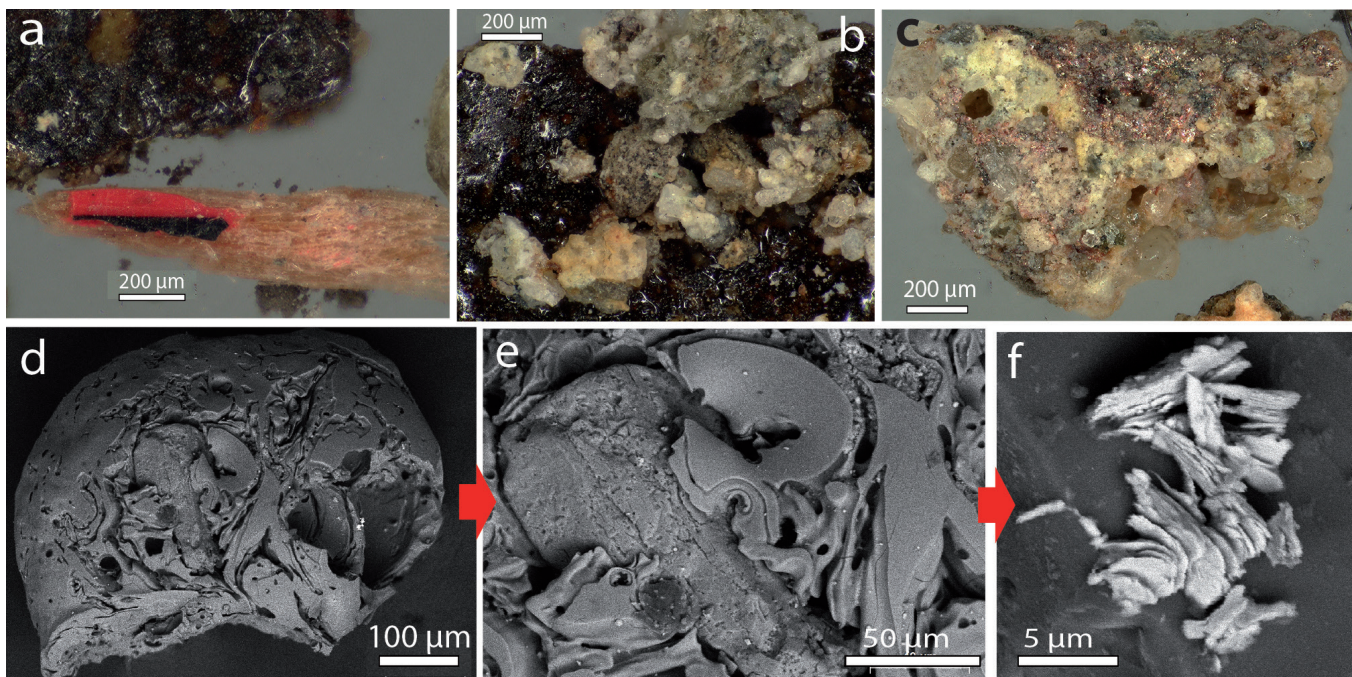


Figure 6 Distinctive features and components of the IIIb microstratified facies. 6a. Residue of a bicolor polymer film sticking to a polymerized reed fragment. 6b. Partly melted vesicular beads sticking to a polymerized carbonaceous aggregate. 6c. Detailed surface view of a vesicular bead with a metal-splashed surface. 6d. SEM view of 6c showing the finely cracked glass matrix with metal inclusions. 6e. Detailed view of 6f showing densely packed FeCrNi nanosheets sticking to the glassy matrix.

of combustion front associated with the charcoal or ash lenses, the scarcity of artefacts, clearly showed that these deposit are not *in situ* firing deposits, neither dumped ashes from hearths and did not suffer trampling. The coupling of siliceous debris beds and silty-clay lenses is typical of occupation surface facies covered with vegetation mats (Figure 9a), very well maintained and allowing only fine dusts to pass through the interstices (Courty and Coqueugniot, 2012). The excellent cohesion of the ash lenses and of the siliceous debris beds demonstrates *in situ* mineralisation by partial decomposition of the biodegradable constituents, either defined as slow self-combustion.

The layered composite ash microfacies (Figure 9b) shows loosely packed lenses of dissociated siliceous residues, pure ashy domains, orange-brown beds consisting of compact silty clay-lime-sandy micro-aggregate domains and fine, rounded, cracked aggregates. Under higher magnification, the fine mass shows an abundance of millime-

tre-sized fragments of fine carbonate clays with plant imprints and calcined domains rich in siliceous debris. In contrast to the microstratified ash facies, the loosely packed lenses of diverse anthropic materials indicate joint deposition of ashes and organic residues from activity areas, of reed-mats and prepared clay materials and their gentle reworking due to partial decomposition and reorganization under compression. The spatial correlations observed in the field between the two types of facies suggests synchronous slow accumulation of organo-mineral residues in a well maintained area and repeated deposition of activity residues in vessels on well-prepared surfaces in the joint area with the high-density of bone and ceramic fragments.

The abundant green aggregates that were retrieved by water sieve from the green coloured microstratified ash deposits showed dense packing of polymerized plant fragments with well-preserved anatomical structure (Figure 9c) embedded in a dense carbonaceous fine mass with pure copper

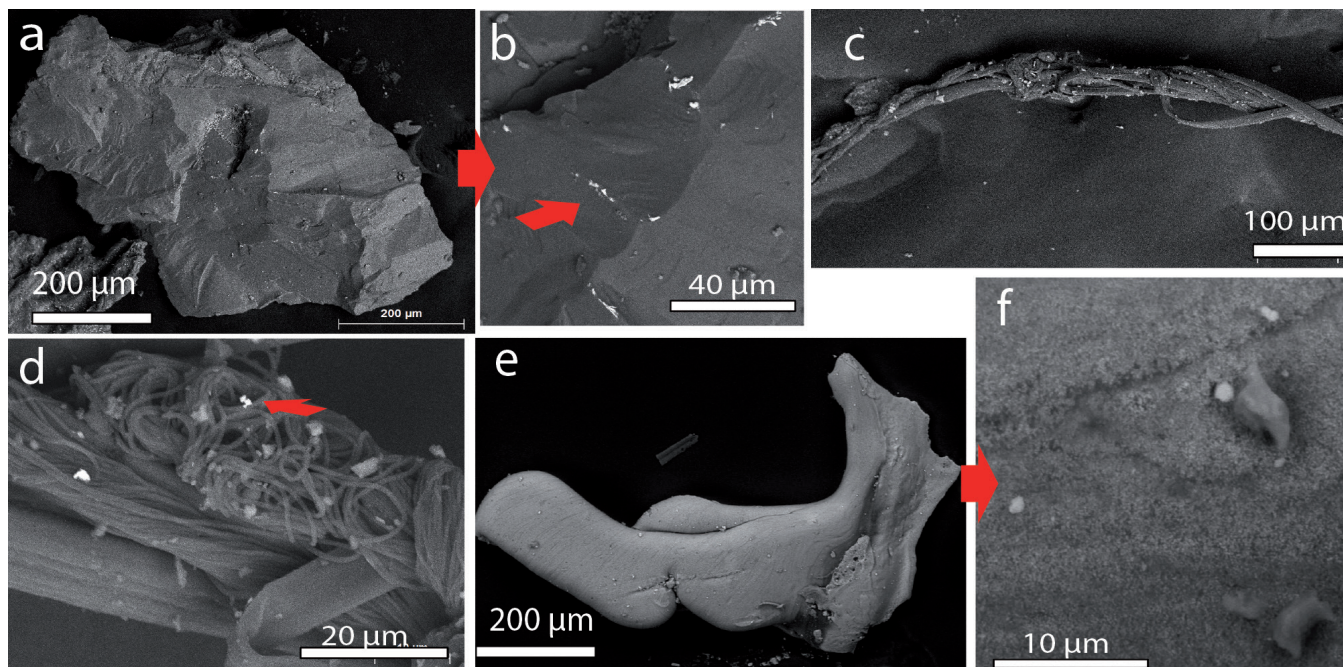


Figure 7 SEM characteristics of distinctive features and components of the IIIb microstratified facies. 7a. Coarse angular quartz with sharp edges. 7b. FeCrNi nanostructured films sticking to the edges of the quartz viewed in Fig. 6a, typical of high energy electric discharge. 7c. Plasma polymer filament formed by electric discharge with its typical twisted morphology. 7d. Detailed view of 7c showing metal incrustations (FeCrNi) within the nanostructured twisted and coiled filaments. 7e. Dense white plasma polymer film formed by electric discharge showing at high magnification (7f) a titanium-rich carbonaceous matrix with TiO_2 microspherules and nanoparticles.

thin film (Figure 9d). Diverse microresidues were extracted from the layered composite ash microfacies, dominantly bone fragments showing metal-rich polymerised coatings, polymer films with metal incrustations, black vesicular volcanic glass and angular quartz with metal coatings and polymerised reed fragments, also with metal inclusions (Figures 9e, 9f and 9g).

The vesicular slag retrieved from the layered composite ash microfacies showed a similar morphology to the vesicular scoriaceous debris of the lower Moche valley unit IIIb deposits. The external surface was smooth, shining, with green metal incrustations looking similar to the polymerised copper metallic domains of the layered composite ash microfacies metallic-looking surface, dotted with granular greenish inclusions (Figure 9h). The fresh break showed a vesicular structure and a

heterogeneous texture characterised by the dense assemblage of micrometric domains of varied composition, particularly carbon-rich coloured domains looking alike the polymer films of the extracted residues from the host matrix (Figure 9i) and abundant nanostructured polymer filaments of diverse colours with metal inclusions. Most of the degassing vesicles were showing under SEM FeCrNi nanostructured films sticking to their sharp edges, a typical deposition of electrically charged metal droplets as previously stated (Figure 9j).

4. Discussion

The wide spatial extent of the different firing deposits across the Moche lower floodplain, their

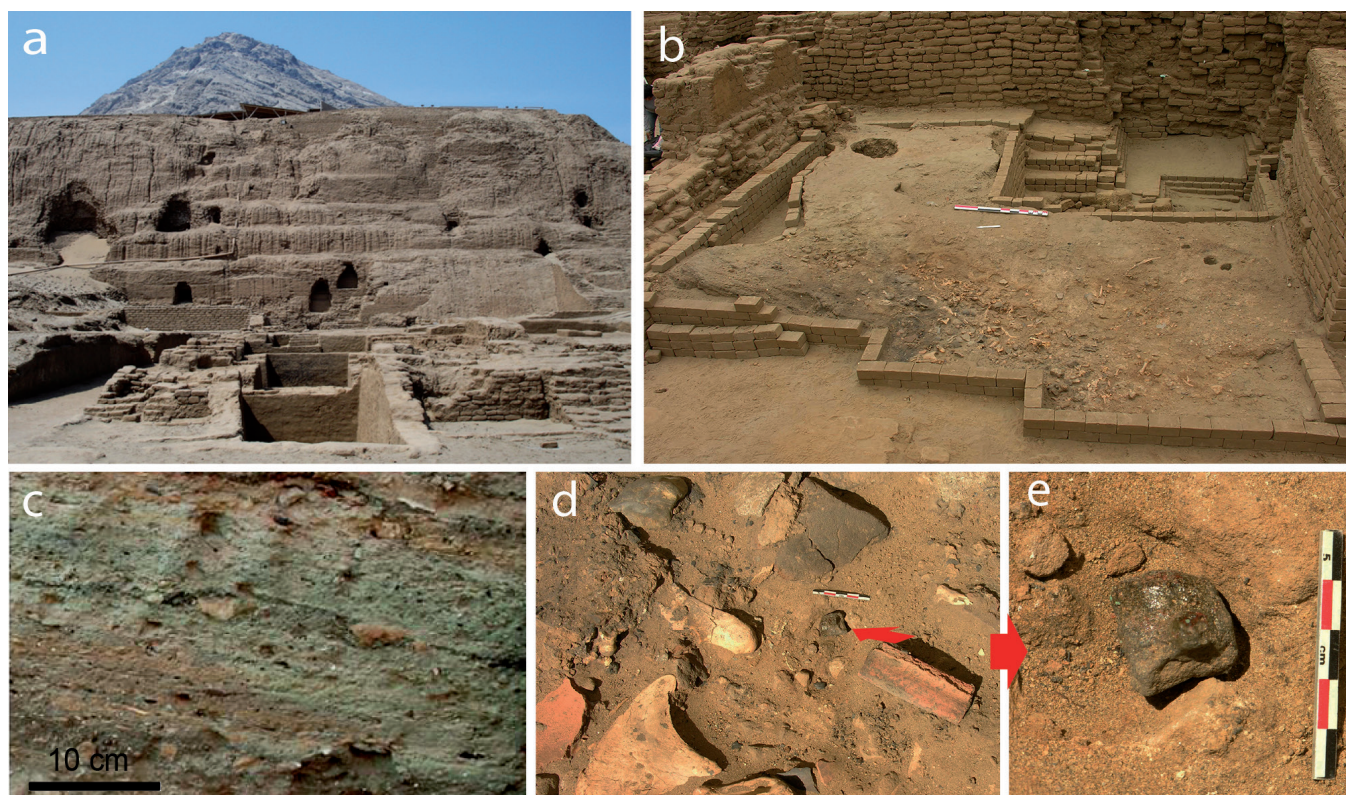


Figure 8 Uhle platform at the foot of the Huaca de la Luna, Moche site. 8a. General view of the excavation of the Uhle platform. 8b. Excavated surface of the layer 21 D occupation complex showing the juxtaposition of stratified ashes and sandy occupation deposits with abundant bone and ceramic fragments. 8c. Densely compacted, greenish, microstratified ashes at the base of the occupation sequence. 8d. Field view of the occupation ritual deposit with in situ fragmented ceramics lying on carbonaceous surfaces, abundant artefacts and a vesicular slag. 8e. Closed view of the slag in its original depositional context.

remarkable preservation and their easy accessibility have offered unique conditions to perform a high-resolution microfacies contextual analysis. Compared to the wide exposure of occupation surfaces in archaeological contexts, the restricted control of the interface integrity could not provide an extensive perception of the different fired surfaces. This was however of major importance to precisely collect the bulk samples from individual

microstrata in order to exactly match the microsequence of depositional events viewed from the thin sections. In agreement to our previous experiences on archaeological firing deposits (Courty *et al.*, 2012, Courty and Coqueugniot, 2013; Courty, 2017; Courty *et al.*, 2020), the micromorphological study of thin sections made from the undisturbed samples was considerably reinforced by the analysis of the residues retrieved from the bulk samples.

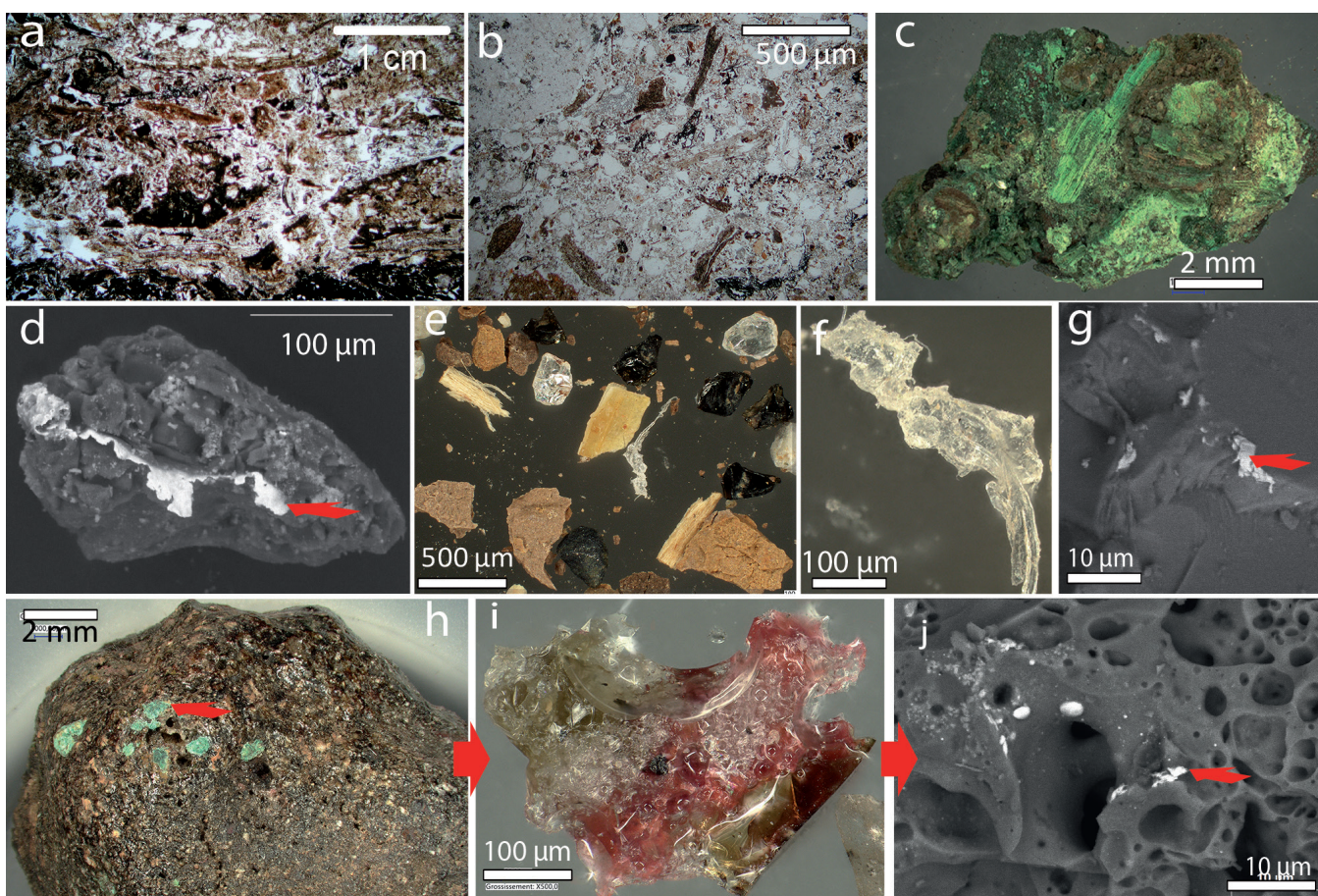


Figure 9 Microfacies and microresidues of the element 21 D layer ritual complex. 9a. Thin-section view of the microstratified ashes formed by the imbrication of siliceous residues rich in phytoliths, thin silty-clay and carbonaceous lenses, typical of prepared surfaces covered by reed-mats. 9b. Thin-section view of the layered composite ash microfacies formed of loosely packed lenses of dissociated siliceous residues, pure ashy domains, orange-brown clayey beds. 9c. Polymerized green aggregates showing superimposition of well-preserved plant fragments in the greenish, microstratified ashes. 9d. SEM view of (8b) showing pure copper thin film within the polymerized matrix. 9e. DSM view of residues from the layered composite ash microfacies: angular quartz, black vesicular volcanic glass, polymer films, polymerised bone fragments, polymerised ashy flakes, polymerised reed fragments. Dull orange, cemented, silty clay formed of iron-oxide rich baked aerosols. 9f. Detailed DSM view of a polymer film. 9g. SEM view of FeCrNi coating on the sharp edges of an aluminosilicate black volcanic glass. 9h. DSM view of the vesicular slag with green incrustations. 9i. Multi-coloured vesicular glass extracted by gentle crushing of the vesicular slag viewed in 9i: the translucent part is formed of silica glass, the red one corresponds to a polymer-rich glass with abundant metal micro and nanoparticles giving the red colour. 9j. SEM view of the vesicular glass showing FeCrNi nanostructured films sticking to the edges of glass vesicles, produced by plasma jet from flash degassing.

The later were particularly crucial to identify the diverse types of polymerised components and their fine integration to the host clay matrix and to the pyroresidues. The use of synthetic resins to impregnate unconsolidated soil-sedimentary materials and as glue films for the thin section preparation introduces polymer filaments of petrochemical origin which are confusing because they morphologically resemble the ones of the firing products. In addition, due to their functionalized surfaces, the polymer filaments interact with the synthetic resins and accumulate in large voids, thus losing in thin section their contextual relevance. This explains why up so far the polymer filaments were considered in micromorphological study as contaminants and were simply ignored (Bullock *et al.*, 1995; Courty *et al.*, 1989).

The DSM analysis of the pyroresidues and of the associated components was also of major help to identify in individual microstrata the joint occurrence of un-charred, charred, calcined and polymerized reed fragments. As previously established (Scott *et al.*, 2017), the mixing of un-charred and charred plants indicates burning of different plant organs and at different temperatures. In addition, the abundance of polymerized flaky reed fragments shows that the sharp silica-rich stems acted as conducting pointy objects at the ground, thus enhancing local charge accumulation and flash-melting by electric arcing (Stolzenburg and Marshall 2021). The occurrence of metal droplets within the polymerized reed surface was crucial to identify the conductive components that were transported from the thundercloud by the hot plasma channel down to the ground, thus contributing to enhance the air conductivity, as well described by Kostinskiy *et al.* (2020).

The DSM residue analysis was even more critically important to identify the systematic presence of these metal droplets on the partly charred and polymerized plant fragments and on the edges of shock-fractured quartz sands in every firing microfacies, without evidence of local melting of the fired surfaces. The rare occurrence in unit IIIb of the vesicular slags with their different composi-

tion from the host matrix and their sharp contact shows that these glassy materials would be more likely aerofulgurites formed in air by agglomeration of electrically charged aerosols and fallen at the ground by gravity fall at the time of intense lightning as observed in recent thunderstorms (Courty and Martínez, 2015).

The similar spatio-temporal pattern of the plasma-formed polymer products showed by the DSM residue analysis for the different firing microfacies thus suggests a common origin from surface propagation of lightning discharges due to the enhanced ground conductivity from the pulverization of electrically charged aerosols.

Although such an aerosol-triggered formation of conductive ground has never been described in present-day lightning situations, this hypothesis matches with the recently proposed scenario of multi-step lightning initiation (Kostinskiy *et al.*, 2020). The wide spatial extent of this ultimate stratified firing deposits across the valley, particularly its regularity and the absence of human artefacts clearly shows a cyclical accumulation by low energy alluvial siltation. These depositional conditions are consistent with a period of prolonged humidity in the upper Andes catchment basin, suggesting high altitude regular precipitation with longlasting recharge of the groundwater aquifers (Gagnon, 2015). These conditions were sufficient to maintain a high moisture content across the flood plain without requiring a seasonal complementary water supply by irrigation canals as previously suspected (Goodbred *et al.*, 2020). The evidence for torrential discharge and interruption of the cyclical regular siltation encountered at the very end of the Moche period clearly express a major environmental change in the Moche flood plain. The Mochica farmers were thus constrained to construct an extensive irrigation network channeling the upland waterflow down to the arable lands of the lower plain in order to maintain their agricultural production.

The complex petrographic composition of the local host soil-sediments in the Moche lower floodplain sequence did not allow to undoubtedly

identify the sources of the exotic components encountered during the episodes of regular alluvial siltation. However, the dominant quartz composition of the local sediments in the layer 21 D occupation complex offers an easier context to identify the exotic components formed of the vesicular volcanic glass with their distinctive metal splashed coatings. The plasma-formed components formed by lightning phenomena are obviously here not in their primary depositional context as they are part of well-prepared occupation floors that were made from the locally available materials. However, this striking abundance of sand-sized vesicular volcanic glass that was only observed in the early occupation deposits incites to suspect that they trace a depositional episode throughout the region of electrically-charged aerosols at this exact time period. The later could potentially originate from volcanic explosive eruptions as suggested by the peak production of electrically-charged aerosols from triboplasma processes in volcanic dust plume (Gaudin and Cimarelli, 2019). This has been recently well illustrated by the exceptionally intense volcanic lightning with lightning flashes in 6 hours with the submarine eruption of Hunga Tonga-Hunga Ha'apai volcano on 2022, January 15th (Yuen *et al.*, 2022). The delayed impact on enhanced atmospheric electrification of the unsteady volcanic plume that transiently reached—at 58 km—the Earth's mesosphere is currently observed across the Earth and should be soon reported.

The record provided both by the Moche lower floodplain deposits and the layer 21 D occupation complex of the lower Moche archaeological sequence would match such a long-distance impact of electrically charged volcanic plume on enhancement of the conductivity at the ground.

The abundance of volcanic glass fragments and the high amount of polymerized plant fragments with their vaporized metal coatings in the later occupation deposits show that the source materials were collected by the Moche people from a soil surface exposed to intense lightning and fall of electrically-charged aerosols. Simply assuming from their depositional context a close link with

ritual human activities, the particular ashy deposits with the vesicular slag would trace an ultimate episode of enhanced atmospheric electrification just synchronous to an early occupational stage, before the construction of the Uhle platform. The fact that these early deposits remained carefully isolated, then protected from architectural remodelling during the successive Moche architectural phases suggests that an ancestral memory of their symbolic relevance was preserved for a few hundred years.

Given the ritual character of this occupation context, the hypothesis of a cultural choice motivated by the desire to leave long-lived food offerings is proposed. The plasma-processes involved in the synthesis of the polymer products give them, in effect, longlasting properties by ionizing-radiation induced crosslinking (Ashfaq *et al.*, 2020). If this hypothesis is correct, it would imply that the Mochicas knew this property of lightning-related durable materials and how to procure the high quality products. There is at present no equivalent in terms of depositional events for a similar type of lightning-related microstratified firing records, neither throughout the successive Moche occupation phases (I to IV), nor in the sand deposits formed during the two recent El Niño events. They all share in common a dominant loose sand texture that is coherent with repeated destabilisation of the coastal sand dunes during this extreme climate conditions which invaded the lower floodplain and the surrounding foothills. The lack of distinctive aeolian sandy deposits at the time of the enhanced electrification events raises critical questions on their environmental and climate relevance. The regular microstratified records for I and III units indicates an overall stability of the floodplain landscapes in spite of the recurrent firing episodes. This could possibly suggest the long-term colonisation of the floodplain by a dense grassland vegetation with would occasionally suffer from severe drying, possibly in response to massive dust storms triggered by long distance volcanic explosions. The exact timing between the final episode of enhanced air conductivity and establishment of the Mochica culture could possibly reveal that

the pyramid builders knew the high quality of the locally available soil resources for raising a durable monumental architecture. Documenting the profusion of polymer components in the clay bricks, the plaster materials and the different pigments used for the wall paintings is beyond the scope of the present-study. However, the marked contrast between the lightning-linked clay-rich materials deposited just before the pyramid construction and the successive sand dune invasion of the monumental architecture shows that the Mochicas had to fight severe drought hazards for maintaining their prosperity.

5. Conclusions and further work

The firing records of the Moche late Holocene floodplain and the close-by early occupation floors formed at the eve of the Mochica colonization raise three major points.

At first, as long established in archaeological sites, the success of an event-based approach for past periods requires (1) well-preserved ancient surfaces associated to microstratified deposits providing an unbiased spatial-temporal records of instantaneous phenomena; (2) a high-resolution multi-analytical protocol aimed to decipher the forming-processes of these pristine surfaces at the finest temporal and spatial scale.

For the first time, the Moche microstratified records show the key role of lightning-triggered droplet pulverization on the instantaneous preservation of firing surfaces, independently of human actions. These atmospheric plasma processes that are comparable to the thin-film plasma coating for surface treatment yet remain to be thoroughly investigated in natural contexts. The instantaneous preservation of organic compounds from the flash-evaporation of volatile gas and the concurrent repolymerization of the most resistant components with the synthesis of filaments and aggregates open new perspective on the key-role of atmospheric electrification on long-term carbon sequestration.

The second major point concerns the identification of different episodes marked by the repeated occurrence of lightning-triggered megafires in an arid region in which this range of extreme events is presently unknown and has never been suspected for past periods. Their similarity in terms of products and effects at the ground suggests that particular atmospheric conditions would be involved in their initiation. The manifestations clearly contrast from the ones of El Niño events that are so far considered as the most threatening climate hazards. In the continuity of the ongoing research on triboelectricity in volcanic plumes (Cimarelli and Genareau, 2021), the Moche valley and site records suggest that electrostatic phenomena in dust clouds could enhance atmospheric electrification and initiate flash-firing events. Obviously, more study is needed to further understand the origin of the precursor particles and the production processes of electrically charged nanoaerosols that are possibly involved in the ongoing marked increased frequency of megafires in North America and Australia.

The final major point relates to the links that we established between ritual activities and the scoria-like glassy slag with the related polymer and metal nanomaterials. In the continuity of the formerly discovered lightning-enhanced fuel flammability (Courty *et al.*, 2020), we hypothesize here that atmospheric electrification phenomena have deeply imprinted the quality of biomass resources and the preservation conditions of organo-mineral residues associated to activity surfaces. Thus, a robust microcontextual study offers the diagnostic key to decode in every living surface the ancestral memories of high-energy manifestations that currently occurred along human history, particularly lightning events. A solid experimental and present-day database of the effects left on the ground in living organisms by electrification phenomena is required to prepare this innovative exploration. The achievements will also greatly help to better monitor the threatening enhancement of atmospheric electrification viewed at present as a direct consequence

of the ongoing global warming (Wang, 2018; Yair, 2018; Williams *et al.*, 2019; Pinto and Pinto, 2020).

Contributions of authors

The author of this article declares that he participated in all its elaboration: conceptualization, data analysis, methodological-technical development, writing of the original manuscript, drafting of the corrected and edited manuscript, graphic design, fieldwork, and interpretation.

Declaration of competing interest

The author declare that she has no known competing financial interests or personal relationships that could have appeared to influence the work reported in this paper.

Financing

The financial support of the French Ministry of foreign Affairs for the excavation conducted at the Uhle Platform, Moche de la Luna Pyramid, is greatly acknowledged. The author is greatly indebted to Claude Chauchat (CNRS, France), director of the Uhle Platform excavation project and to the joint director Belkys Gutiérrez for their full support in the field and their scientific assistance to interpret the archaeological contexts.

The MSH sud (Maison des Sciences de l'Homme-Montpellier) on behalf of the project "Groupe Interdisciplinaire sur l'Electricité Atmosphérique Naturelle (GIEAN)" is greatly acknowledged for its financial support.

Acknowledgments

We are greatly indebted to Prof. Pascal André (LPC-UMR 6533, univ. Clermont, France)

and, to Jean-Michel Martinez (PROMES UPR 8521-UPVD, France) and to Prof. Ahmad Hamdam (département de physique, Université de Montreal, Canada) for sharing their expertise in plasma physics and their scientific support to perform experimentations on effects of electric arcs and plasma discharge.

Conflicts of interest

The author has no conflicts of interest to declare.

References

- Abrahamson, J., Marshall, J., 2002, Permanent electric dipoles on gas-suspended particles and the production of filamentary aggregates: *Journal of electrostatics*, 55(1), 43-63. [https://doi.org/10.1016/s0304-3886\(01\)00183-8](https://doi.org/10.1016/s0304-3886(01)00183-8)
- AghaKouchak, A., Huning, L. S., Chiang, F., Sadegh, M., Vahedifard, F., Mazdiyasni, O., Mallakpour, I., 2018, How do natural hazards cascade to cause disasters?: *Nature*, 561, 458-460. <https://doi.org/10.1038/d41586-018-06783-6>
- Ashfaq, A., Clochard, M. C., Coqueret, X., Dispenza, C., Driscoll, M. S., Ulański, P., Al-Sheikhly, M., 2020, Polymerization reactions and modifications of polymers by ionizing radiation: *Polymers*, 12(12), 2877. <https://doi.org/10.3390/polym12122877>
- Bell, J. E., Brown, C. L., Conlon, K., Herring, S., Kunkel, K. E., Lawrimore, J., Uejio, C., 2018, Changes in extreme events and the potential impacts on human health: *Journal of the Air & Waste Management Association*, 68(4), 265-287. <https://doi.org/10.1080/10962247.2017.1401017>
- Bourget, S., 2016, Sacrifice, violence, and ideology among the Moche: the rise of social complexity in Ancient Peru: USA, University of Texas Press, 463p.
- Babrauskas, V., 2017, Electric arc explosions - A review: *Fire Safety Journal*, 89, 7-15. <http://>

- dx.doi.org/10.1016/j.firesaf.2017.02.006
- Bullock, P., Fedoroff, N., Jongerius, A., Stoops, G., Tursina, T., 1985, Handbook for soil thin section description: International Society of Soil Science, Waine Research, 152p.
- Bunch, T. E., Hermes, R. E., Moore, A. M., Kennett, D. J., Weaver, J. C., Wittke, J. H., DeCarlif, P.S., Bischoff, J.L., Hillman, G., Howardi, G.A., Kimbel, D.R., Kletetschkak, G., Lipom, C.P., Sakaim, S., Revayn, Z., West, A., Firestone, R.B., Kennett, P., 2012, Very high-temperature impact melt products as evidence for cosmic airbursts and impacts 12,900 years ago: Proceedings of the National Academy of Sciences, 109(28), E1903-E1912. <https://doi.org/10.1073/pnas.1204453109>
- Bunch, T. E., LeCompte, M. A., Adedeji, A. V., Wittke, J. H., Burleigh, T. D., Hermes, R. E., Mooney, C., Batchelor, D., Wolbach, W.S., Kathan, J., Kletetschka, G., Patterson, M.C.L., C. Swindel, E.C., Witwer, T., Howard, G.A., Mitra, M., Moore, C.R., Langworthy, K., Kennett, J.P., West, A., Silvia, P.J., 2021, A Tunguska sized airburst destroyed Tall el-Hammam a Middle Bronze Age city in the Jordan Valley near the Dead Sea: Scientific Reports, 11(1), 18632. <https://doi.org/10.1038/s41598-021-97778-3>
- Bychkov, V. L., 2002, Polymer-composite ball lightning: Philosophical Transactions of the Royal Society of London, Series A: Mathematical, Physical and Engineering Sciences, 360(1790), 37-60. <https://doi.org/10.1098/rsta.2001.0918>
- Chauchat, C., Gutierrez, B., Deverly, D., Goepfert, N., 2008, Recherches sur l'élite de la société mochica. La plateforme Uhle à Moche, sur la côte nord du Pérou: Les Nouvelles de l'archéologie, (111/112), 116-122. <https://doi.org/10.4000/nda.433>
- Chauchat, C., Gutiérrez, B., Courty, M.-A., Fontugne, M., Béarez, P., Goepfert, N., Deverly-Louvrier, D., Reveillas, H., Favart, C., Dausse, L., 2021, La plataforma Uhle en Moche Excavaciones 1999-2009: Perú, Instituto Francés de Estudio Andinas (IFEA), 598p.
- Christian, H. J., Blakeslee, R. J., Boccippio, D. J., Boeck, W. L., Buechler, D. E., Driscoll, K. T., Goodman, S.J., Hall, J.M., Koshak, W.J., Mach, D.M., Stewart, M. F., 2003, Global frequency and distribution of lightning as observed from space by the Optical Transient Detector: Journal of Geophysical Research: Atmospheres, 108(D1), ACL-4. <https://doi.org/10.1029/2002JD002347>
- Cimarelli, C., Genareau, K., 2021, A review of volcanic electrification of the atmosphere and volcanic lightning: Journal of Volcanology and Geothermal Research, 107449. <https://doi.org/10.1016/j.jvolgeores.2021.107449>
- Courty, M.-A., 1995, Late quaternary environmental changes and natural constraints to ancient land use (Northwest India), in Johnson, E., (ed.), Ancient peoples and landscapes: Lubbock, Texas, Museum of Texas Tech University, 106-126.
- Courty, M. -A., 2001, Microfacies analysis assisting archaeological stratigraphy, in Goldberg, P., Holliday, V.T., Ferring, C.R., (eds), Earth Sciences and Archaeology: Boston, Springer, 205-239. https://doi.org/10.1007/978-1-4615-1183-0_8
- Courty, M.-A., 2017, Fuel origin and firing product preservation in archaeological occupation contexts: Quaternary International, 431, 116-130, <https://doi.org/10.1016/j.quaint.2015.12.067>
- Courty, M. -A., 2018, Environmental and Societal Memories of Soils, in Berthelin, J., Valentin, C., Charles Munch, J.C., (eds.), Soils as a Key Component of the Critical Zone 1: Functions and Services, 1: USA, Wiley, 275-298. <https://doi.org/10.1002/9781119438069.ch11>
- Courty, M. -A., Allue, E., Henry, A., 2020, Forming mechanisms of vitrified charcoals in archaeological firing-assemblages: Journal of Archaeological Science: Reports,

- 30, 102215. <https://doi.org/10.1016/j.jasrep.2020.102215>
- Courty, M.-A., Goldberg, P., Macphail, R.I., 1989, Soil, micromorphology and archaeology. Cambridge Manuals in Archaeology: United Kingdom, Cambridge University Press, 630p.
- Courty, M.-A., Crisci A., Fedoroff, N., Greenwood, P., Grice, K., Mermoux, M., Smith, D.C., Thiemens, M.R., 2008, Regional manifestation of the widespread disruption of soil-landscapes by the 4 kyr BP impact-linked dust-event using pedo-sedimentary micro-fabrics, in Kapur, S., Mermut, A., Stoops, G. (eds), *New Trends in Soil Micromorphology*: Berlin, Springer, 211-236. https://doi.org/10.1007/978-3-540-79134-8_12
- Courty, M.-A., Carbonell, E., Vallverdú-Poch, J., Banerjee, R., 2012, Microstratigraphic and multi-analytical evidence for advanced Neanderthal pyrotechnology at Abric Romani (Capellades, Spain): *Quaternary International*, 247(9), 294-312. <https://doi.org/10.1016/j.quaint.2010.10.031>
- Courty, M.-A., Coqueugniot, E., 2013, Amicrofacies toolkit for revealing linkages between cultural discontinuities and exceptional geogenic events: the Tell Dja'de case study (NE Syria): *Journal of Archaeological Method and Theory*, 20, 331-362. <https://doi.org/10.1007/s10816-013-9169-4>
- Courty, M.-A., Martinez J.-M., 2015, Terrestrial carbonaceous debris tracing atmospheric hypervelocity-shock aeroplasm processes: *Procedia Engineering*, 103, 81-88. <https://doi.org/10.1016/j.proeng.2015.04.012>
- DeMenocal, P. B., 2001, Cultural responses to climate change during the late Holocene: *Science*, 292(5517), 667-673. <https://doi.org/10.1126/science.1059287>
- Dillehay, T., Kolata, A.L., Pino, M., 2004, Pre-industrial human and environment interactions in northern Peru during the late Holocene: *Holocene* 14, 272-281. <https://doi.org/10.1191/0959683604hl704rp>
- Essene, E.J, Fisher, D.C., 1986, Lightning strike fusion: extreme reduction and metal-1662 silicate liquid immiscibility: *Science* 234,189-93. <https://doi.org/10.1126/science.234.4773.189>
- Feng, T., Lang, C., Pasek, M. A., 2019, The origin of blue coloration in a fulgurite from Marquette, Michigan: *Lithos*, 342, 288-294. <https://doi.org/10.1016/j.lithos.2019.06.003>
- Gagnon, C. M., Andrus, C. F. T., Ida, J., Richardson, N., 2015, Local water source variation and experimental Chicha de Maíz brewing: Implications for interpreting human hydroxyapatite δ^{18} values in the Andes: *Journal of Archaeological Science: Reports*, 4, 174-181. <https://doi.org/10.1016/j.jasrep.2015.09.008>
- Gaudin, D., Cimarelli, C., 2019, The electrification of volcanic jets and controlling parameters: A laboratory study: *Earth and Planetary Science Letters*, 513, 69-80. <https://doi.org/10.1016/j.epsl.2019.02.024>
- Gifford, A. C., 1999, Clay soil fulgurites in the Eastern Goldfields of Western Australia: *Journal of the Royal Society of Western Australia*, 82, 165-168.
- Goodbred Jr, S. L., Dillehay, T. D., Mora, C. G., Sawakuchi, A. O., 2020, Transformation of maritime desert to an agricultural center: Holocene environmental change and landscape engineering in Chicama River valley, northern Peru coast: *Quaternary Science Reviews*, 227, 106046. <https://doi.org/10.1016/j.quascirev.2019.106046>
- Grapes, R. H., Müller-Sigmund, H., 2010, Lightning-strike fusion of gabbro and formation of magnetite-bearing fulgurite, Cornone di Blumone, Adamello, Western Alps, Italy: *Mineralogy and Petrology*, 99(1-2), 67-74. <https://doi.org/10.1007/s00710-009-0100-3>
- Hamdan, A., Kabbara, H., Courty, M. A., Cha, M. S., Martinez, J. M., Belmonte, T., 2017, Synthesis of carbon-metal multi-strand nanocomposites by discharges in heptane

- between two metallic electrodes: *Plasma Chemistry and Plasma Processing*, 37(4), 1069-1090. <https://doi.org/10.1007/s11090-017-9816-8>
- Holliday, V. T., Bartlein, P.J., Scott, A. C., Marlon, J. R., 2020, Extraordinary biomass-burning episode and impact winter triggered by the Younger Dryas cosmic impact ~12,800 years ago, parts 1 and 2: a discussion: *The Journal of Geology*, 128(1), 69-94. <https://doi.org/10.1086/706264>
- Humbert, L., 1972, Atlas de pétrographie des systèmes carbonatés: Paris, Technip.
- Izhovkina, N. I., Artekha, S. N., Erokhin, N. S., Mikhailovskaya, L. A., 2020, Electrostatic Disturbances of Aerosol Atmospheric Plasma: Beaded Lightning: *Pure and Applied Geophysics*, 177(11), 5475-5482. <https://doi.org/10.1007/s00024-020-02568-z>
- James, M. R., Wilson, L., Lane, S.J., Gilbert, J. S., Mather, T. A., Harrison, R. G., Martin, R. S., 2008, Electrical charging of volcanic plumes: *Space Science Reviews*, 137(1), 399-418. <https://doi.org/10.1007/s11214-008-9362-z>
- Khaykin, S., Legras, B., Bucci, S., Sellitto, P., Isaksen, L., Tence, F., Bekki, S., Bourassa, A., Rieger, L., Zawada, D., Jumelet, J., Godin-Beekmann, S., 2020, The 2019/20 Australian wildfires generated a persistent smoke-charged vortex rising up to 35 km altitude: *Communications Earth & Environment*, 1(1), 1-12. <https://doi.org/10.1038/s43247-020-00022-5>
- Kim, S. M., Yoo, Y. W., Lee, B. H., 2016, Discharge characteristics in soils subjected to lightning impulse voltages: *Journal of Electrical Engineering and Technology*, 11(2), 446-454. <https://doi.org/10.5370/JEET.2016.11.2.446>
- Kolata, A. L., Binford, M. W., Brenner, M., Janusek, J. W., Ortloff, C., 2000, Environmental thresholds and the empirical reality of state collapse: A response to Erickson (1999): *Antiquity*, 74(284), 424-426. <https://doi.org/10.1017/S0003598X00059512>
- Kostinskiy, A. Y., Marshall, T. C., Stolzenburg, M., 2020, The Mechanism of the origin and development of lightning from initiating event to initial breakdown pulses (v. 2): *Journal of Geophysical Research: Atmospheres*, 125(22), e2020JD033191. <https://doi.org/10.1029/2020JD033191>
- Lockard, G. D., 2009, The occupational history of Galindo, Moche Valley, Peru: *Latin American Antiquity*, 20(2), 279-302. <https://doi.org/10.1017/S1045663500002649>
- Liu, Y., Williams, E., Li, Z., Guha, A., LaPierre, J., Stock, M., Heckman, S., Zhang, Y., DiGangi, E., 2021, Lightning Enhancement in Moist Convection with Smoke-laden Air Advected from Australian Wildfires: *Geophysical Research Letters*, 48(11), e2020GL092355. <https://doi.org/10.1029/2020GL092355>
- Lushnikov, A. A., Zagaynov, V. A., Lyubovtseva, Y. S., Gvishiani, A. D., 2014, Nanoaerosol formation in the troposphere under the action of cosmic radiation: *Izvestiya, Atmospheric and Oceanic Physics*, 50(2), 152-159. <https://doi.org/10.1134/S0001433814020078>
- Moore, A. M., Kennett, J. P., Napier, W. M., Bunch, T. E., Weaver, J. C., LeCompte, M., Adedeji, V., Hackley, P., Kletetschka, G., Hermes, R.E., Wittke, J.H., Razink, J.J., Gaultois, M.W., West, A., 2020, Evidence of cosmic impact at Abu Hureyra, Syria at the Younger Dryas Onset (~ 12.8 ka): High-temperature melting at > 2200 C.: *Scientific Reports*, 10, 4185. <https://doi.org/10.1038/s41598-020-60867-w>
- Moseley, M. E., Keefer, D. K., 2008, Deadly deluges in the southern desert: Modern and ancient El Niños in the Osmore region of Peru, in Sandweiss, D., Quilter, G., (eds.) *El Niño, Catastrophism, and Culture Change in Ancient America*: Washington D.C., Dumbarton Oaks Research Library and Collection, 129-44.
- Murphy, A., 2020, Lightning strike direct effects, in Irving, P., Soutis, C., (eds.), *Polymer Composites in the Aerospace Industry: USA*,

- Woodhead Publishing, 561-591. <https://doi.org/10.1016/B978-0-08-102679-3.00018-6>
- Nna Mvondo, D., Navarro-González, R., McKay, C. P., Coll, P., Raulin, F., 2001, Production of nitrogen oxides by lightning and coronae discharges in simulated early Earth, Venus and Mars environments: *Advances in Space Research*, 27(2), 217-223. [https://doi.org/10.1016/S0273-1177\(01\)00050-3](https://doi.org/10.1016/S0273-1177(01)00050-3)
- ONERN, 1973, *Inventario, evaluación y uso racional de los recursos naturales de la costa: Cuenca del Rio Moche*: Lima, Oficina Nacional de Evaluación de Recursos Naturales, 532p.
- Pasek, M. A., Block, K., Pasek, V., 2012, Fulgurite morphology: a classification scheme and clues to formation: *Contributions to Mineralogy and Petrology*, 164(3), 477-492. <https://doi.org/10.1007/s00410-012-0753-5>
- Pasek, M. A., Pasek, V. D., 2018, The forensics of fulgurite formation: *Mineralogy and Petrology*, 112(2), 185-198. <https://doi.org/10.1007/s00710-017-0527-x>
- Pinto Jr, O., Pinto, I. R., 2020, Lightning changes in response to global warming in Rio de Janeiro, Brazil: *American Journal of Climate Change*, 9(3), 266-273. <https://doi.org/10.4236/ajcc.2020.93017>
- Rodbell, D. T., Seltzer, G. O., Anderson, D. M., Abbott, M. B., Enfield, D. B., Newman, J. H., 1999, An ~15,000-year record of El Niño-driven alluviation in southwestern Ecuador. *Science*, 283(5401), 516-520. <https://doi.org/10.1126/science.283.5401.516>
- Sandweiss, D. H., Richardson III, J.B., 2008, Central Andean Environments, in Silverman, H., Isbell, W.H., (eds.), *Handbook of South American Archaeology*: New York, Springer, 93 – 104. https://doi.org/10.1007/978-0-387-74907-5_6
- Scott, A. C., Hardiman, M., Pinter, N., Anderson, R. S., Daulton, T. L., Ejarque, A., Finch P., Carter-champion, A., 2017, Interpreting palaeofire evidence from fluvial sediments: a case study from Santa Rosa Island, California, with implications for the Younger Dryas Impact Hypothesis: *Journal of Quaternary Science*, 32(1), 35-47. <https://doi.org/10.1002/jqs.2914>
- Stolzenburg, M., Marshall, T. C., 2021, The role of grounded conducting pointy objects during Thunderstorm Ground Enhancements (TGEs): arXiv. <https://doi.org/10.48550/arXiv.2108.04138>
- Swain, D. L., Singh, D., Touma, D., Diffenbaugh, N. S., 2020, Attributing extreme events to climate change: A new frontier in a warming world: *One Earth*, 2(6), 522-527. <https://doi.org/10.1016/j.oneear.2020.05.011>
- Tedim, F., Leone, V., Amraoui, M., Bouillon, C., Coughlan, M. R., Delogu, G. M., Fernandes, P.M., Ferreira, C., McCaffrey, S., McGee, T.K., Parente, J., Paton, D., Pereira, M.G., Ribeiro, L.M., Viegas, D.X., Xanthopoulos, G., 2018, Defining extreme wildfire events: difficulties, challenges, and impacts: *Fire*, 1(1), 9. <https://doi.org/10.3390/fire1010009>
- Tierney, J. E., Poulsen, C. J., Montañez, I. P., Bhattacharya, T., Feng, R., Ford, H. L., Honisch, B., Inglis, G.N., Petersen, S.V., Sagoo, N., Tabor, C.R., Thirumalai, K., Zhu, J., Burls, N.J., Godderis, Y., Foster, G.L., Huber, B.T., Ivany, L.C., Turner, S.K., Lunt, D.J., McElwain, J.C., Mills, B.J.W., Otto-Bliesner, B.L., Ridgwell, A., Zhang, Y.G., 2020, Past climates inform our future: *Science*, 370(6517). <https://doi.org/10.1126/science.aay3701>
- Yair, Y., 2018, Lightning hazards to human societies in a changing climate: *Environmental Research Letters*, 13(12), 123002. <https://doi.org/10.1088/1748-9326/aaca86>
- Veraverbeke, S., Rogers, B. M., Goulden, M. L., Jandt, R. R., Miller, C. E., Wiggins, E. B., Randerson, J. T., 2017, Lightning as a major driver of recent large fire years in North American boreal forests: *Nature Climate Change*, 7(7), 529-534. <https://doi.org/10.1038/NCLIMATE3329>
- Wang, Q., Li, Z., Guo, J., Zhao, C., Cribb,

- M.,2018, The climate impact of aerosols on lightning: Is it detectable from long-term aerosol and meteorological data? : *Atmospheric Chemistry and Physics*, 18, 12797–12816. <https://doi.org/10.5194/acp-18-12797-2018>
- Williams, E., Guha, A., Boldi, R., Christian, H., Buechler, D., 2019: Global lightning activity and the hiatus in global warming: *Journal of Atmospheric and Terrestrial Physics*, 189, 27–34. <https://doi.org/10.1016/j.jastp.2019.03.011>
- Waylen, P.R., Caviedes, C.N., 1986, El Niño and annual floods on the north Peruvian littoral: *Journal of Hydrology*, 89(1-2), 141-156. [https://doi.org/10.1016/0022-1694\(86\)90148-4](https://doi.org/10.1016/0022-1694(86)90148-4)
- Wolbach, W.S., Ballard, J.P., Mayewski, P.A., Parnell, A.C., Cahill, N., Adedeji, V., Bunch, T.E., Domínguez-Vázquez, G., Erlandson, J.M., Firestone, R.B., French, T.A., Howard, G., Israde-Alcántara, G., Johnson, J.R., Kimbel, D., Kinzie, C.R., Kurbatov, A., Kletetschka, G., LeCompte, M.A., Mahaney, W.C., Melott, A.L., Mitra, S., Maiorana-Boutilier, A., Moore, C.R., Napier, W.M., Parlier, J., Tankersley, K.B., Thomas, B.C., Wittke, J.H., West, A., Kennett, J.P., 2018, Extraordinary biomass-burning episode and impact winter triggered by the Younger Dryas cosmic impact ~12,800 years ago. 1. ice cores and glaciers: *The Journal of Geology*, 126(2), 185-205. <https://doi.10.1086/695703>
- Yuen, D. A., Scruggs, M. A., Spera, F. J., Zheng, Y., Hu, H., McNutt, S. R., Thompson, G., Mandli, K., Kellerf, B.R., Wei, S.S., Peng, Z., Zhou, Z., Mulargia, F., Tanioka, Y.,2022, Under the surface: Pressure-induced planetary-scale waves, volcanic lightning, and gaseous clouds caused by the submarine eruption of Hunga Tonga-Hunga Ha’apai volcano: *Earthquake Research Advances*, 2(3), 100134. <https://doi.org/10.1016/j.eqrea.2022.100134>